Multi-GPU based 3D numerical modeling of fluid migration and clay dehydration influence on Lusi hydrothermal activity (Java, Indonesia)

Reza Sohrabi, Benjamin Malvoisin, Adriano Mazzini, Stephen Miller

Multi-GPU based 3D numerical modeling of fluid migration and clay dehydration influence on Lusi hydrothermal activity (Java, Indonesia)

Reza Sohrabi [a,*], Benjamin Malvoisin [b], Adriano Mazzini [c], Stephen A. Miller [a]

[a] Centre for Hydrogeology and Geothermics (CHYN), University of Neuchâtel, Neuchâtel, Switzerland

[b] Institut des Sciences de la Terre (ISTerre), Université Grenoble Alpes, CNRS, Grenoble, France

[c] Centre for Earth Evolution and Dynamics (CEED), University of Oslo, Oslo, Norway

[*]Corresponding author. E-mail address: reza.sohrabi@unine.ch (R. Sohrabi)

Keywords: High-Performance Computing (HPC); Graphics Processing Unit (GPU); 3D numerical modeling; Lusi; Hydrothermal system

Highlights:

- Couplings between fluid flow, heat transport and reactions in the Lusi system solved with multi-GPU technology
- High-Performance Computing with 3D numerical models using multi-GPU processing
- Fluid pressure build-up due to clay dehydration controls hydrothermal system fluid outflow

Abstract

The Lusi mud eruption in East Java has been active since May 2006. Magma emplacement at depth, clay dehydration, and mud liquefaction during seismic wave propagation have been invoked as mechanisms fueling this eruption. However, the respective roles of these processes are still poorly constrained. In this focused study, we numerically investigate the influence of clay dehydration, mass and heat transport on fluid outflow at the Lusi site using a fully coupled 3D model for this active system. Using a multi-GPU parallel processing algorithm, we propose an estimate of the 3D time evolution of pressure, temperature, porosity, permeability and water liberation in a large-scale (9 km - 14 km - 5.5 km) deep hydrothermal system at high-resolution. Simulations indicate that high-pressure fluids generated by dehydration reactions are sufficient to induce hydro-fractures that would significantly influence the porosity and permeability structures. Dehydration is an essential component for understanding the Lusi system, because the fluids generated contribute to the outflow and may have a considerable impact for the maintenance of the infrastructure required to keep the Lusi site safe. High-Performance Computing (HPC) offers high-resolution simulations for studying time evolution of such natural systems, and potentially for geothermal resource development for the surrounding population.

1 Introduction

3D numerical modeling is a powerful tool for investigating processes occurring in the Earth's interior such as hydrothermal circulation or geothermal exploitation. The dynamics of such complex systems involve coupled and nonlinear flow, heat transport and reaction. Quantitative analysis of these systems is challenging and relies on numerical solutions of coupled partial differential equations (PDEs). Considerable effort during the last decades focused on various algorithms for solving PDEs on multi-CPU platforms, but these algorithms have made limited use of evolving hardware changes such as GPU-computing. 3D numerical modeling of hydrothermal systems presents a major challenge due to the physical processes involved (Ingebristen et al., 2010; Jeanne et al., 2014) over both short and long-terms (White, 1957; Bowen, 1979; Ingebritsen & Sanford, 1999; Lowenstern & Hurwitz, 2008; Hurwitz & Manga, 2017). Scientific models have been developed for heat and mass transport through porous media with progressively more complex physics (White & Oostrom, 2003; Steefel et al., 2005; Bangerth et al., 2007; Zhang et al., 2008; Gaston et al., 2009; Flemisch et al., 2011; Kolditz et al., 2012; Hammond et al., 2014; Su et al., 2017). The need for predictive tools led to the development of reactive models considering reaction kinetics and reaction induced changes in porosity (Steefel et al., 2005; Lichtner & Carey, 2006; Lichtner & Kang, 2007; Xu et al., 2008). However, none of these have used multi-GPU technology.

The Lusi eruption (Java, Indonesia) provides an unprecedented opportunity to test large scale numerical modeling for a hydrothermal system at its infancy. This system, erupting since the 29th of May 2006 in East Java, elicited debate in science and politics (Van Noorden, 2006). During the early phases, a sequence of aligned clastic eruptions appeared through fractures that followed the same orientation as the Watukosek fault system, a NE-SW tectonic structure in NE Java (Figure 1). This structure can be observed from satellite images and exhibits fractures (including antithetic lineaments), in the field and on seismic data (Mazzini et al., 2009; Moscariello et al., 2018; Obermann et al., 2018; Sciarra et al., 2018; Mazzini et al., 2021). Fluids quickly flooded large parts of the Sidoarjo Regency urban area, permanently displacing 60,000 people (Richards, 2011). Fifteen years later, Lusi continues to erupt boiling mud breccia and displays perpetual geyser-like behavior (Karyono et al., 2017) with flow rates of ~ 80,000 m^3/day and, with significant earthquake-triggered increases, up to ~120,000 m^3/day (Miller and Mazzini, 2018; Mazzini et al., 2021). This system displays complex interactions between hydrothermal fluids and carbonate- and clay-rich formations in an active tectonic setting neighboring a volcanic complex.

Numerical modeling helps decipher the mechanisms involved in Lusi hydrothermal system formation and evolution. Mud flow is generally studied by considering a mud reservoir linked to the

surface by a mud filled conduit. Zoporowski and Miller (2009) reproduced the oscillatory behavior of the eruption with such a geometry. Rudolph et al. (2011) considered the effect of overpressure in the mud reservoir on flow through the conduit, and eruption longevity. Davies et al. (2011) also estimated the evolution of the eruption rate with time but with a probabilistic approach. Collignon et al. (2018) determined the influence of conduit radius and clast presence on flow velocity in the conduit. Numerical modeling was also used at Lusi to study other processes than mud flow. Istadi et al. (2009) studied the surface area affected by the eruption by combining topographic data with measured mud flow while considering processes such as faulting and subsidence. Svensen et al. (2018) used a one-dimensional thermal model to predict the influence of magma emplacement at depth on the emission of CO_2. Mazzini et al. (2009) studied the link between strike-slip faulting and fluidization with several rheological models. Tanikawa et al. (2010) modelled the generation of overpressure during diagenesis. All these models shed light on processes involved in the eruption. However, three-dimensional models were not developed, preventing the complex geological structure observed at Lusi (Mazzini et al., 2007) from being reproduced. Moreover, the contribution of heated fluids generated by magmatic intrusion emplacement and clay dehydration is still enigmatic.

This study investigates the evolution of the Lusi system by exploring hydrothermal fluid circulation and coupled hydro-thermo-mechanical interactions and its potential use for geothermal resources. We report on a series of numerical simulations using multi-GPU computing to model physical processes involved in this eruptive clastic system. We show that evolution of the Lusi hydrothermal eruption is likely connected to the generation of high fluid pressures by dehydration reactions as proposed by Mazzini et al. (2007, 2012, 2018) and petrographic data analyses (Malvoisin et al., 2018; Zaputlyaeva et al., 2020). These authors revealed that the clasts originating from the deepest sedimentary formation (i.e. Ngimbang Formation shale source rock) intersected by the Lusi conduit have been exposed to temperatures higher than 350°C. However, the Ngimbang Formation sediments have never been included in any numerical simulation representing the Lusi system. Our modeling shows that dehydration can generate a substantial overpressure and the fluids necessary to support eruption at Lusi. Our model represents the first attempt to model the couplings between reaction, deformation and fluid flow at high-resolution. Here we present a novel approach using models developed to simulate more than 7 billion numerical grid cells in a relatively short computational time (less than a week).

We explore this hypothesis with two different scenarios where in magmatic intrusion and related hydrothermal fluid migration at depth (500°C and 1,000°C beneath Lusi) induces dehydration within the sediment package and, ultimately, we quantify this contribution to the overall fluid

outflow. Finally, we investigate the influence of simple reactions and temperature changes on porosity and fluid pressure to determine the evolution of fluid flow. The investigation of this complex system requires the development of long-term computational multi-physics approaches at high-resolution in three dimensions.

2 Methodology and model set-up

The local stratigraphy has been constrained from borehole data complemented by regional studies, seismic data interpretations, and analysis of erupted clasts (Mazzini et al., 2007; Malvoisin et al., 2018; Moscariello et al., 2018; Samankassou et al., 2018; Zaputlyaeva et al., 2020). The identified units and formations have been used by Sohrabi et al. (2018) to propose the first 3D geological model for the Lusi eruption: Altered sand, shale and clay from the Pucangan Formation (blue) in Figure 2a, Bluish Grey clay from the Upper Kalibeng Formation (purple), volcanoclastics from the Upper Kalibeng Formation (red), carbonates from the Kujung-(Prupuh)/Tuban Formations (orange), and mudstones from the Ngimgbang Formation (yellow). The model also includes two major faults or shear zones (red) crossing Lusi, the Watukosek strike slip system and the Siring antithetic faults system (Figure 2a). This 3D heterogeneous geological numerical model is then implemented in a newly developed numerical High-Performance Computing (HPC) tool for subsurface fluid dynamics (Sohrabi et al., 2019). To our knowledge, there is no other numerical tool that can couple physical processes such as clay dehydration, considering porosity and permeability evolution through time, in three-dimensions at such high-resolution (more than 7 billion numerical cells).

Lusi is a sediment-hosted hydrothermal system connected at depth with a neighboring magmatic complex located ~10 km to the SW (Miller and Mazzini, 2018). Geochemical studies show that Lusi vents a mixture of gases that indicate formation temperatures of up to 400 °C (Mazzini et al., 2012). Measurements reveal that Lusi represents one of the largest natural gas systems on Earth, with CH_4 emissions up to 0.1 Tg/year and CO_2 release comparable to large volcanic systems (Mazzini et al., 2021). High helium isotopic ratios, with mantle-derived signature, have been measured from the gas collected at Lusi (R/Ra = 7) and are those measured at the fumaroles of the neighboring volcanic complex (R/Ra = 7.3) (Mazzini et al., 2012; Inguaggiato et al., 2018; Sciarra et al, 2018). Regional tomography studies reveal that the Lusi conduit is connected at 4.5 km depth with the volcanic complex through a magmatic intrusion/hydrothermal fluids migration propagating towards the NE of Java Island (Fallahi et al., 2017). In agreement with these evidences, studies completed on clast erupted from the Lusi crater, reveal that they had been exposed to temperatures >350 °C, inconsistent with the local geothermal gradient extrapolated to the apparent source depth (Malvoisin et al., 2018; Zaputlyaeva et al., 2020).

Accordingly, for our modeling, we consider an additional heat source supplied by magmatic intrusion and related hydrothermal fluid migration at depth supplementing the initial conductive geothermal gradient of 42°C/km measured prior to the eruption (Mazzini et al., 2007). The model does not include magma flow and dynamics, only the added heat source, assumed to be at a depth of 5.5 km. We investigate two scenarios, one with fluid temperature at 500°C, consistent with a linear interpolation of the thermometry data obtained on clasts erupted at Lusi (Malvoisin et al. 2018; Zaputlyaeva et al., 2020), and the second with fluid temperature of 1,000°C, that considers a non-linear temperature evolution with depth. The surface temperature is set to 27°C (Svensen et al., 2018). For rock properties, we used the parameters found in Svensen et al. (2018) for the lithology, combined with analyses from Mazzini et al. (2012) and Tanikawa et al. (2010). We assume that the flow properties of supercritical CO_2 are similar to those of water because supercritical CO_2 is ten times more compressible than water, but it is also about ten times less viscous (Miller et al., 2004). This allows modeling fluid flow by considering only one fluid phase, which is a valid assumption for most of the modeling domain except near the surface where gas forms. This may have consequences on temperature estimates at shallow depth because the latent heat of vaporization is not incorporated in the heat conservation equation. Because we consider a one-phase H_2O-CO_2 mixture, mud transport is not simulated. Clay dehydration and mass and heat transport in porous media are linked to porosity and permeability changes, which may affect outflow at the surface. Dehydration reactions involve large and sometimes rapid volume changes related to free water release from the clay mineralogical structure. They occur not only during diagenesis but also as a result of pressure and temperature increase during metamorphism (Vidal and Dubacq, 2009). The reaction of the two main clay layers (Upper Kalibeng Formation and Ngimgbang Formation) (Figure 2b) may thus change the thermo-hydrodynamic properties of the sediment-hosted Lusi system.

2.1 Physical model

The aim of our work is to model the impact of clay dehydration on the Lusi fluid flow. Modeling the complex couplings between reaction, fluid flow and deformation is usually performed with pre-existing codes (e.g. Xu et al., 2011). However, the achievable resolution using such models is low (approximately several thousands of grid cells; Izadi and Elsworth, 2013; Shabani et al., 2020), precluding the inclusion of complex geological structures. Fluid migration and flow at Lusi are apparently controlled by the Watukosek Fault system (Mazzini et al., 2009) so that it is essential to use at least moderately high-resolution. To attain such definition, the physical model is simplified in an effort to highlight processes playing a first-order role on fluid flow at Lusi (dehydration, heating,

permeability evolution). The approach presented here does not use separate modules to implement reaction, fluid flow and deformation, and instead fully coupled fluid pressure and porosity variations are calculated in single equations (Malvoisin et al., 2015). We use a continuum porous media approach and solve the governing nonlinear equations with the Finite Difference (FD) method. Clay dehydration reactions can play a significant role in the evolution of porosity and permeability and may also contribute to over-pressure development. Production of fluid through dehydration reactions establishes pore pressure gradients that then must diffuse to the surroundings. Mazzini et al. (2007, 2018) measured lower salinity in the fluids expelled at Lusi than in seawater, and attributed this dilution to clay dehydration based on enrichment in B, Li and ^{18}O and a depletion in ^{2}H in the expelled fluids. Analyses on side well cores from the BJP1 borehole, located in the vicinity of Lusi, revealed that illite-smectite transformation (a dehydration reaction) occurs in the sediments of the Bluish Grey clays from the Upper Kalibeng Formation (Mazzini et al., 2007).

We model the temperature-dependent clay dehydration by fitting the water content/temperature curve found in Vidal & Dubacq (2009) for the illite-smectite transformation. We use the 3D geological model proposed by Sohrabi et al. (2018) to generate a distribution of porosity and permeability, and the 3D multi-GPU simulator developed by Sohrabi et al. (2019) for clay dehydration.

2.1.1 Mass conservation

We compute fluid pressure (*Pf*), temperature (*T*), porosity (ϕ) , permeability (*k*), and fluid generation from clay dehydration as follows.

Total mass conservation in a porous and reacting medium is:

$$\frac{\partial(\rho_f \phi + \rho_s(1-\phi))}{\partial t} + \nabla \cdot \left(\rho_f \phi v_f + \rho_s(1-\phi)v_s\right) = 0 \quad (1)$$

where ϕ, ρ, v are the porosity (volume fraction of fluid), density and velocity, respectively, and subscripts '*s*' and 'f ' denote the properties of the solid and the fluid. Mass of nonvolatile species is conserved by (Malvoisin et al., 2015):

$$\frac{\partial(\rho_s(1-X_s)(1-\phi))}{\partial t} + \nabla \cdot (\rho_s(1-X_s)(1-\phi)v_s) = 0 \quad (2)$$

where the amount of fluid into the solid X_s is calculated at the equilibrium with a fit of the data of Vidal and Dubacq (2009), which gives X_s as a function of temperature in the smectite/illite system.

2.1.2 Conservation of momentum

Conservation of fluid momentum is expressed by Darcy's law:

$$\phi(v_f - v_s) = -\frac{k_0 \phi^3}{\mu_f}(\nabla P_f - \rho_f g) \quad (3)$$

where the permeability (k) is related to the porosity through the Kozeny-Carman relationship with an exponent 3 and a constant background permeability k_0 (Kozeny, 1927; Carmen, 1937; Carmen, 1956), μ_f is the fluid viscosity, g is the gravitational constant, and P_f is the fluid pressure.

The fluid pressure considering the effects of clay dehydration on volume change (rock density ρ_s constant without viscous deformation) can be expressed as (Malvoisin et al., 2015):

$$\nabla \frac{k_0 \phi^3}{\mu_f}\left(\nabla P_f - \rho_f g\right) = \beta_{eff} \frac{dP_f}{dt} + \left(1 - \frac{\rho_s}{\rho_f}\right) \cdot \frac{1-\phi}{1-X_s} \cdot \frac{dX_s}{dt} \quad (4)$$

where the partial time derivatives are replaced by material derivatives ($\frac{d}{dt} = \frac{\partial}{\partial t} + \nabla v_s$) and β_f and β_s are the fluid and pore (crack) compressibility. The effective compressibility β_{eff} is described by:

$$\beta_{eff} = \beta_f + \frac{\beta_s}{1-\phi} \quad (5)$$

The hydro-mechanical porosity change due to fluid production by metamorphism can be expressed by (Malvoisin et al., 2015):

$$\frac{d\phi}{dt} = \beta_s \frac{dP_f}{dt} - \frac{(1-\phi)}{(1-X_s)} \cdot \frac{dX_s}{dt} \quad (6)$$

2.1.3 Energy conservation

Energy heat conservation over an elemental volume of medium (solid and fluid phase) at thermal equilibrium so that $T = T_s = T_f$ (Nield & Bejan, 2006) is:

$$\Big((1-\phi)\rho_s c_s + \phi\big(\rho_f c_f\big)\Big)\frac{\partial T}{\partial t} + \big(\rho_f c_f\big) v_f \cdot \nabla T = \nabla \cdot \Big(\big((1-\phi)\lambda_s + \phi\lambda_f\big)\nabla T\Big) + \big((1-\phi)q_s + \phi q_f\big) \quad (7)$$

where c is the specific heat of the phase, λ is the thermal conductivity and q is the heat production per unit volume. Equations 1 to 7 results in a highly nonlinear system of differential equation solved here by using the Finite Deference (FD) method.

The general coupled parameters used for simulations are shown in Table 1. Parameter values chosen for the fully coupled 3D numerical model (Table 1) are inputs measured and calculated from previous studies.

Table 1: Parameters definition and values used.

Symbol	Definition	Parameters	Units
$\boldsymbol{P_f}$	Fluid pressure	-	Pa
$\boldsymbol{\rho_f}$	Density of fluid	-*	kg·m^{-3}
$\boldsymbol{\rho_s}$	Density of solid	2650	kg·m^{-3}
$\boldsymbol{v_f}$	Velocity of fluid	-	m·s^{-1}
$\boldsymbol{\beta_f}$	Compressibility of fluid	1e^{-10}	Pa^{-1}
$\boldsymbol{\beta_s}$	Compressibility of solid	1e^{-9}	Pa^{-1}
$\boldsymbol{\beta_{eff}}$	Effective Compressibility	-	Pa^{-1}
$\boldsymbol{\phi}$	Porosity	-	-
$\boldsymbol{k}$	Permeability	-	m^2
$\boldsymbol{X_s}$	Mass fraction of fluid in solid	-	wt %
T	Temperature	-	°C
$\boldsymbol{c_f}$	Fluid specific heat	4190	J/kg·K
$\boldsymbol{c_s}$	Solid specific heat	1000	J/kg·K
$\boldsymbol{\lambda_f}$	Fluid thermal conductivity	0.6	W/ m·K
$\boldsymbol{\lambda_s}$	Solid thermal conductivity	2.1	W/ m·K
$\boldsymbol{q_f}$	Fluid heat production	-	J/ m^3/ s
$\boldsymbol{q_s}$	Solid heat production	-	J/ m^3/ s
$\boldsymbol{g}$	Gravity acceleration	9.81	m^{2}s^{-1}

* calculated with the Equation of State (EOS) from Sun et al. (2008).

3. Results

We generated a numerical grid for multi-GPU computing from the 3D geological model (Figure 3). We performed 3D simulations in space and time to quantify the effects of clay dehydration in the Upper Kalibeng (purple) and the Ngimgbang (yellow) Formations. We numerically investigated two scenarios with different heated fluid temperatures (500°C and 1,000°C). Time zero was chosen as the onset of the fluid eruption in 2006. Figures 4 and 5 show the calculated parameters through the shear zones/faults as pressure (P_f), temperature (T), porosity (ϕ), permeability (k) and the quantity of fluid (X_s).

We simulated up to 200 years of the system evolution. However, we present only the first 50 years of simulation because fluids produced by dehydration are expected to mostly exhausted by this time. The temperature distributions for the two considered scenarios are different (Figure 4a and Figure 5a). We observe over pressure in the Upper Kalibeng clay Formation of up to 5-10 MPa (Figure 4b and Figure 5b). Through the 50 years of simulation, we perceive that the Ngimgbang and the Upper Kalibeng Formations liberate ~ 17 % and ~ 40 % of their stored water, respectively. This amount of water release modifies the porosity and the permeability of the shear zones/faults (Figure 4c, d and Figure 5c, d). Figure 4e and Figure 5e show that clay layers had already been largely dehydrated by diagenesis before Lusi started to erupt (e.g. illization, Mazzini et al., 2007).

Figure 6 and Figure 7 show the evolution of the temperature through the entire Lusi system. These calculated temperatures do not represent the fluid temperature at shallow depth, because two important shallow physical processes are not considered in this work. The latent heat of vaporization, as already discussed, is not implemented neither is the meteoritic and groundwater recharge in the system. Both these processes are extremely efficient in significantly dropping the fluid temperatures of the active system at shallow depths. Figure 8 and Figure 9 show the porosity through the two shear zones/faults (Watukosek and Siring faults) during 50 years of activity. We observe that the temperature of fluid source (500°C or 1,000°C) does not strongly modify the overall temperature distribution in the system over this time scale. The system comes to equilibrium after a certain time. The calculated porosity evolution shows that a 500°C fluid source generates less change in the rock properties of the Ngimgbang Formation than in the Upper Kalibeng Formation.

We computed the amount of fluid released from the two different clay layers (Upper Kalibeng and Ngimgbang Formation) after Lusi began to erupt (Figure 10). The Upper Kalibeng Formation releases four times (~ 4x) more water than the Ngimgbang Formation. Simulated results within the first decade overestimate by a factor of ~ 2 to 3 the measured outflow of fluids at the Lusi site (Mazzini et al., 2007; Mazzini et al., 2012). The simulated volume of water released is 240,000

m^3/day for a fluid source at 1,000°C and 230,000 m^3/day for fluids at 500°C during the first decade. Simulated outflow caused by clay dehydration was around 60,000 m^3/day after 25 years and 343 m^3/day after 50 years for a fluid source at 1,000°C. Using instead 500°C, simulated water release was around 51,000 m^3/day after 25 years and 184 m^3/day after 50 years. After 25 years, the temperature in the conduit (Watukosek and Siring faults intersection) is constant at depths greater than ~ 1,500 m (Figure 4a and Figure 5a). As a result, fluid production in the two clay layers ceases (Figure 4e and Figure 5e).

4. Discussion

4.1 Hydrothermal system of Lusi: evolution and lifetime

We investigated the influence of a high-temperature intrusion/hydrothermal fluids migration at depth on clay dehydration, using a high-resolution 3D numerical model. We integrate previous field data measurements and calculations (Mazzini et al., 2007; Mazzini et al., 2012; Mazzini, 2018). Results show that dehydration from two clay layers will continue to drive the Lusi system. The model proposed here invokes clay dehydration after ascent of hot fluids from a deep source. This process was suggested by geochemical measurements (Mazzini et al., 2007; Mazzini et al., 2012; Malvoisin et al., 2018) and we demonstrate here that it can explain aqueous fluid ascent and eruption at Lusi. Flow dynamics controlled by hot fluid ascent may partly reproduce a geyser behaviour, even though the Lusi pulsations are not predicted here (Mazzini et al., 2007; Zoporowski and Miller, 2009; Karyono et al., 2017; Lupi et al., 2018). Geysering is “almost” always associated with multiphase flow. The fact that it does not occur in these simulations probably reflects, at least in part, the single-phase approximation. The Lusi system is of potential resource interest on the long term, regardless the initial temperature of the fluid source. The simulations show fluid flow mainly controlled by the highly permeable pathways provided by fault/shear zones, and these could be targeted for geothermal energy.

Model simulations show that dehydration of the underlying clay layers around ~ 1,500 m (Upper Kalibeng Formation) and ~ 5,000 m (Ngimgbang Formation) could release additional fluid in the future. We investigated two scenarios, and both overestimate by a factor of 2-3x fluid production when compared with on-site measurements. However, these measurements only considered outflow from the main vents (Mazzini et al., 2021) and do not include the large quantities of water released from other active vents.

Our model considers one fluid phase and does not implement the latent heat of vaporization. It is thus unable to model vaporization and its effect on temperature. After magma emplacement at

depth, the temperature progressively increases towards the surface up to values above 100°C after 10 years of simulated eruption (Figure 5). The lack of heat extraction due to vaporization also induces temperature overestimation at depth after 10 years of simulated eruption. This effect is more pronounced near the surface, that is in the Upper Kalibeng Formation rather than in the Ngimgbang Formation. The main objective of our model is to investigate the effect of clay dehydration on fluid dynamics at Lusi. Dehydration is complete in the Ngimgbang Formation in the first 10 years of the eruption. Two thirds of the maximum dehydration and of the porosity increase also occur in the Upper Kalibeng Formation during this period (Figure 5c and Figure 5e). Neglecting vaporization in our model thus only affects one third of the predicted dehydration after 10 years of eruption in the Upper Kalibeng Formation. Vaporization will induce cooler temperature in this formation than predicted with the model. This will slow down its dehydration. The duration of the eruption of 50 years predicted here is thus a minimum. The amount of liberated fluid could also be overestimated by a maximum of one third since vaporization could also reduce the maximum temperature reached in the Upper Kalibeng Formation during the eruption.

Water liberation through dehydration calculated here depends in part on the uncertainties associated with the 3D geological model. Further, the physics applied here do not consider the effect of reaction on heat budget (Eqs. 1 to 7), the influence of boiling, or possible cooling by meteoric water. This explains why the results found in Figure 4a and Figure 5a greatly overestimate shallow temperature in the shear zones/faults zone at later simulation times. The overly high simulated temperatures may also explain why the extent of dehydration in the Upper Kalibeng Formation is 15% higher in the model (82% of dehydration) than in the natural samples (65% illitization; Mazzini et al., 2007). Groundwater recharge from the sediment-hosted system and fluid flow in the shallow surface linked to the Arjuno-Welirang volcanic complex should also be considered in future simulations, to encompass the hydrogeological complexity of the region.

This is the first 3D computational model of the Lusi's mud eruption that estimates the contribution of clay dehydration to fluid generation at depth (Figure 11). However, it considers single-phase flow of an aqueous fluid. This approximation is justified at depth greater than ~ 1,800 m, since large part of the mud is believed to originate in the Upper Kalibeng Formation (Mazzini et al., 2007). As mud is more viscous than pure aqueous fluid, this may lead to overestimation of fluid velocity in the top part of our model. Zoporowski and Miller (2009), Rudolph et al. (2011) and Collignon et al. (2018) investigated mud flow between the mud source and the surface with single-phase, two-dimensional models considering mud as a viscous fluid. However, the impact of interplay between the various phases is still poorly constrained. This hampers our ability to accurately predict flow dynamics, especially near the surface where mud and aqueous fluid coexist and gas can form. Developing a

multi-phase numerical model of Lusi should thus be targeted for future numerical investigation. Further, even though our model provides more complete treatment of the geological complexity at Lusi, it does not solve for stress evolution. We consider the influence of the Watukosek Fault System on permeability but do not model fluidization and subsidence associated with faulting, which is known to play a key role on fluid dynamics at Lusi (Istadi et al., 2009; Mazzini et al., 2009; Osorio et al., 2021). Finally, other processes may deserve to be considered for in future large-scale numerical modeling; including thermal maturation of organic matter in contact with a magmatic intrusion at depth (Svensen et al., 2018), and focusing of seismic waves, which may favor fluidization (Lupi et al., 2013; Lupi et al., 2014).

If, in the future, we see a notable increase of the geothermal gradient across the entire sediment-hosted hydrothermal system of East Java, we will have to recalculate and re-estimate the initial conditions invoked in our simulations. In addition, if the fluid outflow at the Lusi site does not decrease on a decadal scale, we might infer that the fluid discharging from the Lusi vent is recharged by other sources.

4.2 Implications for potential geothermal resources

Hydrothermal systems can be found in many places and used as geothermal energy resources, as in Italy (e.g. Lardarello), Iceland (e.g. Blue Lagoon), and the U.S.A. (e.g. The Geysers). Each of these systems has a specific hydrogeological environment and its own complexity. At Lusi dehydration may be an important element. The Salton Sea (California, U.S.A.), a sediment-hosted hydrothermal system (Svensen et al., 2007; Mazzini et al., 2011), may bear some resemblance to Lusi (Mazzini et al., 2018). However, Salton Sea system has been geologically active for a long while compared to Lusi. There, deep heated fluids fill the system and structural clay dehydration causes porosity evolution at a different scale. Our results show that for 50 years following the Lusi inception in 2006, the dynamics and thermodynamics will be strongly dependent on this process, which induces irreversible physical changes to the rock via water release.

Our high-resolution 3D numerical simulations track the controlled rock property changes (dehydration) over 50 years. The models suggest that the clay dehydration should decrease after 25 years and may stop after 50 years. The complex volcanic structure in the vicinity of Lusi is a potential source of geothermal energy for the surrounding population as reflected by the simulation distribution of temperature in time and space (Figure 6 and Figure 7). The simulations suggest evolving property profiles which may control hydro-thermo-mechanical structure over time.

5. Conclusions

We present 3D numerical simulations using multi-GPU computing of fluid thermo-hydrodynamics with porosity and permeability evolution driven by hydrothermal fluid intrusion at 5.5 km depth below the active Lusi eruption. Starting from 2006, the results demonstrate that Lusi decreasing less outflow due to decreasing clay dehydration (in the Upper Kalibeng Formation and Ngimgbang Formation) over the next decade. Our simulations suggest that the contribution of dehydration to water release may essentially stop after 25 years of activity and completely stop after 50 years.

Clay mineral illitization, already ongoing before the eruption, continues mainly in the Upper Kalibeng Formation but also in the Ngimgbang Formation under conditions of increasing temperature and pressure. This process is irreversible and may be complete after about 50 years. The simulations are consistent with the degree of illitization measured on site. Heating of the Upper Kalibeng Formation could produce hydro-fractures which will enhance a preferential pathway for fluid to the surface. Porosity and permeability evolution in time can have a non-negligible effect.

The Lusi activity may still persist after 50 years because of the groundwater recharge of the entire hydrothermal system linked to the Arjuno-Welirang volcanic complex.

The initial temperature of the source fluids (500°C or 1,000°C) does not have a significant influence on the entire system. Temperatures are better reproduced during the first decade of Lusi activity with a hypothetic source at 500°C. The 10 MPa calculated overpressure calculated and the heated fluids coming from 5.5 km are primary controls on the clay dehydration rates.

3D numerical modeling can inform decision making on natural or engineered systems. High-Performance Computing (HPC) is a valuable technique to model physical processes in a reasonable computational time. Geothermal reservoir valorization is an important topic today. Decisions have to be made regarding use of renewable energy. Deeper boreholes and complementary coupled numerical physical analyses are needed to evaluate this potentially large geothermal energy supply.

Acknowledgements

We appreciate helpful discussions with G. Jansen, Y.Y. Podladchikov and B. Valley. We thank the Editor and anonymous reviewers for very constructive suggestions.

Competing interests

The authors declare that they have no known competing financial interests or personal relationships that could have appeared to influence the work reported in this paper.

Funding

This work was funded by a grant from the Swiss National Science Foundation (SNSF) Project n°200021-16005/1 and by the European Research Council under the European Union's Seventh Framework Programme Grant agreement No. 308126 (LUSI LAB project) and the Research Council of Norway through its Centers of Excellence funding scheme, Project number 223272 (CEED) and the HOTMUD Project number 288299

Data availability

The relevant data to reproduce the numerical results are provided in the manuscript. The remaining data used in this study are available from cited references. All data and materials that support the findings of this study can be made available, in some form, to any researcher for purposes of reproducing or extending the analysis upon reasonable request to the corresponding author R.S.

Code availability

The numerical code used in this study is available from cited reference (with restrictions) upon reasonable request.

Figure captions

Figure 1: a) Inset map of Indonesia and topographic map showing the Arjuno-Welirang volcanic complex to the south with some of the surrounding hydrothermal springs. Lusi and other mud volcanoes are located to the north of the island inside the sedimentary basin. b) Aerial image showing erupting craters in the central part of the inaccessible hydrothermal pond.

Figure 2: Conceptual model for fluid pressure increase controlled by dehydration in a deep hydrothermal system or geothermal reservoir. Under conditions of increasing temperature and pressure, clay dehydration reactions begin. a) 3D conceptual model considering five main stratigraphic units and two main shear zone/faults at Lusi site. b) 3D model set-up for simulations, considering deep heated fluids filling the entire Lusi hydrothermal system.

Figure 3: 3D structural numerical grid with initial parameters permeability (k) and porosity (ϕ) distribution at high-resolution (384x384x384) for multi-GPU calculation. This numerical grid is based on the 3D geological model of Lusi presented in Sohrabi et al. (2018).

Figure 4: Evolution of simulated a) temperature, b) pressure, c) porosity, d) permeability and e) water liberation through the Lusi shear zones/faults after fluid intrusion at 500°C after: 0 years (red), 5 years (green), 10 years (blue), 25 years (magenta) and 50 years (dashed cyan).

Figure 5: Evolution of simulated a) temperature, b) pressure, c) porosity, d) permeability and e) water liberation through the Lusi shear zones/faults after fluid intrusion at 1,000°C after: 0 years (red), 5 years (green), 10 years (blue), 25 years (magenta) and 50 years (dashed cyan).

Figure 6: Evolution of temperature from an initial geothermal gradient of 42°C/km throughout the system and fluid intrusion at 500°C with input parameters presented in the 3D geological model (Figure 3). Times are since Lusi erupted.

Figure 7: Evolution of temperature from an initial geothermal gradient of 42°C/km throughout the system and fluid intrusion at 1,000°C with input parameters presented in the 3D geological model (Figure 3). Times are since Lusi erupted.

Figure 8: Evolution of porosity after fluid intrusion at 500°C with input parameters presented in the 3D geological model (Figure 3). The two shear zones/faults are shown with a focus on the two clay layers (Upper Kalibeng Formation and Ngimgbang Formation). Times are since Lusi erupted.

Figure 9: Evolution of porosity after fluid intrusion at 1,000°C with input parameters presented in the 3D geological model (Figure 3). The two shear zones/faults are shown with a focus on the two clay layers (Upper Kalibeng Formation and Ngimgbang Formation). Times are since Lusi erupted.

Figure 10: Release water due to the dehydration of the two main clay layers over 50 years after Lusi started to erupt in 2006. The red line shows results for the fluid intrusion at 1,000 °C and the blue line results for fluid intrusion at 500 °C. The green circles are outflow data measured at the Lusi vent.

Figure 11: Conceptual model based on the numerical simulations performed in this work. Heated fluids associated with magmatic intrusion at depth induces clay dehydration feeding the Lusi mud eruption.

References

Bangerth, W., Hartmann, R., Kanschat, G. (2007). Deal. II-a general purpose object-oriented finite element library. ACM transactions on Mathematical Software (TOMS). 33(4), 24

Bowen, Robert. (1979). Geothermal resources. London: New York: Applied Science Publishers; Halsted Press

Carman, P. C. (1937). Fluid flow through granular beds. Transactions-Institution of Chemical Engineeres, 15, 150-166.

Carman, P. C. (1956). Flow of gases through porous media. Academic press.

Collignon, M., Schmid, D. W., Galerne, C., Lupi, M., & Mazzini, A. (2018). Modelling fluid flow in clastic eruptions: Application to the Lusi mud eruption. Marine and Petroleum Geology, 90, 173-190.

Davies, R. J., Mathias, S. A., Swarbrick, R. E., & Tingay, M. J. (2011). Probabilistic longevity estimate for the LUSI mud volcano, East Java. Journal of the Geological Society, 168(2), 517-523.

Fallahi, M. J., Obermann, A., Lupi, M., Karyono, K., & Mazzini, A. (2017). The plumbing system feeding the Lusi eruption revealed by ambient noise tomography. Journal of Geophysical Research: Solid Earth, 122(10), 8200-8213.

Flemisch, B., Darcis, M., Erbertseder, K., Faigle, B., Lauser, A., Mosthaf, K., Müthing, S., Nuske, P., Tatomir, A., Wolff, M., Helmig, R. (2011). DuMux: DUNE for multi-{phase,component,scale, physics,…} flow and transport in porous media. Adv. Water Resour. 34(9), 1102–1112

Gaston, D., Newman, C., Hansen, G., Lebrun-Grandie, D. (2009). MOOSE: a parallel computational framework for coupled systems of nonlinear equations. Nucl. Eng. Des. 239(10), 1768–1778

Hammond, G.E., Lichtner, P.C., Mills, R.T. (2014). Evaluating the performance of parallel subsurface simulators: an illustrative example with PFLOTRAN. Water Resour. Res. 50(1), 208–228

Hurwitz, S., & Manga, M. (2017). The fascinating and complex dynamics of geyser eruptions. Annual Review of Earth and Planetary Sciences, 45, 31-59.

Inguaggiato, S., Mazzini, A., Vita, F., & Sciarra, A. (2018). The Arjuno-Welirang Volcanic Complex and the connected Lusi system: geochemical evidences. Marine and Petroleum Geology, 90, 67-76.

Ingebritsen, S. E., & Sanford, W. E. (1999). Groundwater in geologic processes. Cambridge University Press.

Ingebritsen, S. E., Geiger, S., Hurwitz, S., & Driesner, T. (2010). Numerical simulation of magmatic hydrothermal systems. Reviews of Geophysics, 48(1).

Istadi, B. P., Pramono, G. H., Sumintadireja, P., & Alam, S. (2009). Modeling study of growth and potential geohazard for LUSI mud volcano: East Java, Indonesia. Marine and Petroleum Geology, 26(9), 1724-1739.

Izadi, G., & Elsworth, D. (2013). The effects of thermal stress and fluid pressure on induced seismicity during stimulation to production within fractured reservoirs. Terra Nova, 25(5), 374-380.

Jeanne, P., Rutqvist, J., Vasco, D., Garcia, J., Dobson, P. F., Walters, M., & Borgia, A. (2014). A 3D hydrogeological and geomechanical model of an Enhanced Geothermal System at The Geysers, California. Geothermics, 51, 240-252.

Karyono, K., Obermann, A., Lupi, M., Masturyono, M., Hadi, S., Syafri, I., Abdurrokhim, A., & Mazzini, A., (2017). Lusi, a clastic-dominated geysering system in Indonesia recently explored by surface and subsurface observations: Terra Nova, v. 29, p. 13-19

Kolditz, O., Bauer, S., Bilke, L., Böttcher, N., Delfs, J.O., Fischer, T., et al. (2012). OpenGeoSys: an open source initiative for numerical simulation of thermo-hydro-mechanical/chemical (THM/C) processes in porous media. Environ. Earth Sci. 67(2), 589–599

Kozeny, J. (1927). Uber kapillare leitung der wasser in boden. Royal Academy of Science, Vienna, Proc. Class I, 136, 271-306.

Lichtner, P.C., Carey, J.W. (2006). Incorporating solid solutions in reactive transport equations using a kinetic discrete-composition approach. Geochimica et Cosmochimica Acta. 70(6), 1356–1378

Lichtner, P.C., Kang, Q. (2007). Upscaling pore-scale reactive transport equations using a multiscale
continuum formulation. Water Resources Research. 43, W12S15

Lowenstern, J. B., & Hurwitz, S. (2008). Monitoring a supervolcano in repose: Heat and volatile flux at the Yellowstone Caldera. Elements, 4(1), 35-40.

Lupi, M., Saenger, E., Fuchs, F., Miller S.A. (2013). Lusi mud eruption triggered by geometric focusing of seismic waves. Nature Geoscience, 6, 642–646.

Lupi, M., Saenger, E. H., Fuchs, F., & Miller, S. A. (2014). Correction: Corrigendum: Lusi mud eruption triggered by geometric focusing of seismic waves. Nature Geoscience, 7(9), 687-688.

Lupi, M., Mazzini, A., Sciarra, A., Collignon, M., Schmid, D. W., Husein, A., ... & Karyono, K. (2018). Enhanced hydrothermal processes at the new-born Lusi eruptive system, Indonesia. Journal of Volcanology and Geothermal Research, 366, 47-57.

Malvoisin, B., Podladchikov, Y. Y., & Vrijmoed, J. C. (2015). Coupling changes in densities and porosity to fluid pressure variations in reactive porous fluid flow: Local thermodynamic equilibrium. Geochemistry, Geophysics, Geosystems, 16(12), 4362-4387.

Malvoisin, B., Mazzini, A., & Miller, S. A. (2018). Deep hydrothermal activity driving the Lusi mud eruption. Earth and Planetary Science Letters, 497, 42-49.

Mazzini, A., Svensen, H., Akhmanov, G. G., Aloisi, G., Planke, S., Malthe-Sørenssen, A., & Istadi, B. (2007). Triggering and dynamic evolution of the LUSI mud volcano, Indonesia. Earth and Planetary Science Letters, 261(3), 375-388.

Mazzini, A., Nermoen, A., Krotkiewski, M., Podladchikov, Y., Planke, S., & Svensen, H. (2009). Strike-slip faulting as a trigger mechanism for overpressure release through piercement structures.

565 Implications for the Lusi mud volcano, Indonesia. Marine and Petroleum Geology, 26(9), 1751-
566 1765.
567
568 Mazzini, A., Svensen, H., Etiope, G., Onderdonk, N., & Banks, D. (2011). Fluid origin, gas fluxes
569 and plumbing system in the sediment-hosted Salton Sea Geothermal System (California,
570 USA). Journal of Volcanology and Geothermal Research, 205(3-4), 67-83.
571 Mazzini, A., Etiope, G., & Svensen, H., (2012). A new hydrothermal scenario for the 2006 Lusi
572 eruption, Indonesia. Insights from gas geochemistry: Earth and Planetary Science Letters, v. 317-
573 318, p. 305-318.
574
575 Mazzini, A. (2018). 10 years of Lusi eruption: Lessons learned from multidisciplinary studies
576 (LUSI LAB).
577
578 Mazzini, A., Scholz, F., Svensen, H. H., Hensen, C., & Hadi, S. (2018). The geochemistry and
579 origin of the hydrothermal water erupted at Lusi, Indonesia. Marine and Petroleum Geology, 90, 52-
580 66.
581
582 Mazzini, A., Sciarra, A., Etiope, G., Sadavarte, P., Houweling, S., Pandey, S., and Husein, A.
583 (2021). Relevant methane emission to the atmosphere from a geological gas manifestation:
584 Scientific Reports, v. 11, no. 1, p. 4138.
585
586 Miller, S. A., Collettini, C., Chiaraluce, L., Cocco, M., Barchi, M., & Kaus, B. J. (2004).
587 Aftershocks driven by a high-pressure CO 2 source at depth. Nature, 427(6976), 724.
588
589 Miller, S. A. & Mazzini, A. (2018). More than ten years of Lusi: A review of facts, coincidences,
590 and past and future studies. Marine and Petroleum Geology, 90, 10-25.
591
592 Moscariello, A., Do Couto, D., Mondino, F., Booth, J., Lupi, M., & Mazzini, A. (2018). Genesis and
593 evolution of the Watukosek fault system in the Lusi area (East Java). Marine and Petroleum
594 Geology, 90, 125-137.
595
596 Nield, D. A. & Bejan, A. (2006). Convection in porous media (Vol. 3). New York: springer.
597
598 Obermann, A., Karyono, K., Diehl, T., Lupi, M., and Mazzini, A. (2018). Seismicity at Lusi and the
599 adjacent volcanic complex, Java, Indonesia: Marine and Petroleum Geology, v. 90, p. 149-156.

Richards, J. R. (2011). Report into the past, present, and future social impacts of Lumpur Sidoarjo. Humanitus Sidoarjo Fund.

Osorio Riffo, Á., Mauri, G., Mazzini, A., and Miller, S. A. (2021). Tectonic insight and 3-D modelling of the Lusi (Java, Indonesia) mud edifice through gravity analyses: Geophysical Journal International, v. 225, no. 2, p. 984-997.

Rudolph, M. L., Karlstrom, L., & Manga, M. (2011). A prediction of the longevity of the Lusi mud eruption, Indonesia. Earth and Planetary Science Letters, 308(1-2), 124-130.

Samankassou, E., Mazzini, A., Chiaradia, M., Spezzaferri, S., Moscariello, A., & Do Couto, D. (2018). Origin and age of carbonate clasts from the Lusi eruption, Java, Indonesia. Marine and Petroleum Geology, 90, 138-148.

Sciarra, A., Mazzini, A., Inguaggiato, S., Vita, F., Lupi, M., & Hadi, S. (2018). Radon and carbon gas anomalies along the Watukosek fault system and Lusi mud eruption, Indonesia. Marine and Petroleum Geology, 90, 77-90.

Shabani, B., Pashin, J., & Vilcáez, J. (2020). TOUGHREACT-CO2 Bio–A new module to simulate geological carbon storage under biotic conditions (Part 2): The bio-geochemical reactive transport of CO2-CH4-H2-H2S gas mixtures. Journal of Natural Gas Science and Engineering, 76, 103190.

Sohrabi, R., Jansen, G., Malvoisin, B., Mazzini, A., & Miller, S. A. (2018). Numerical modeling of the Lusi hydrothermal system: Initial results and future challenges. Marine and Petroleum Geology, 90, 191-200.

Sohrabi, R., Omlin, S., & Miller, S. A. (2019). GEYSER: 3D thermo-hydrodynamic reactive transport numerical simulator including porosity and permeability evolution using GPU clusters. Computational Geosciences, 23, 1317-1330.

Steefel, C.I., DePaolo, D.J., Lichtner, P.C. (2005). Reactive transport modelling: an essential tool and a new research approach for the earth sciences. Earth Planet. Sci. Lett. 240(3–4), 539–558

Su, D., Mayer, K.U., MacQuarrie, K.T. (2017). Parallelization of MIN3PTHCm: a high-performance computational framework for subsurface flow and reactive transport simulation. Environ. Model Softw. 95, 271–289

Sun, H., Feistel, R., Koch, M., Markoe, A. (2008). New equations for density, entropy, heat capacity, and potential temperature of a saline thermal fluid. Deep-Sea Res. I Oceanogr. Res. Pap. 55(10), 1304 - 1310.

Svensen, H., Karlsen, D. A., Sturz, A., Backer-Owe, K., Banks, D. A., & Planke, S. (2007). Processes controlling water and hydrocarbon composition in seeps from the Salton Sea geothermal system, California, USA. Geology, 35(1), 85-88.

Svensen, H. H., Iyer, K., Schmid, D. W., & Mazzini, A. (2018). Modelling of gas generation following emplacement of an igneous sill below LUSI, east Java, Indonesia. Marine and Petroleum Geology, 90, 201-208.

Tanikawa, W., Sakaguchi, M., Wibowo, H. T., Shimamoto, T., & Tadai, O. (2010). Fluid transport properties and estimation of overpressure at the Lusi mud volcano, East Java Basin. Engineering Geology, 116(1), 73-85.

Van Noorden, R. (2006). Mud volcano floods Java. Nature.

Vidal, O., & Dubacq, B. (2009). Thermodynamic modelling of clay dehydration, stability and compositional evolution with temperature, pressure and H2O activity. Geochimica et Cosmochimica Acta, 73(21), 6544-6564.

White, D. E. (1957). Thermal waters of volcanic origin. Geological Society of America Bulletin, 68(12), 1637-1658.

White, M.D., Oostrom, M. (2003). STOMP subsurface transport overmultiple phases version 3.0 user's guide (No. PNNL-14286). Pacific Northwest National Lab., Richland, WA

Xu, T., Spycher, N., Sonnenthal, E., Zhang, G., Zheng, L., & Pruess, K. (2011). TOUGHREACT Version 2.0: A simulator for subsurface reactive transport under non-isothermal multiphase flow conditions. Computers & Geosciences, 37(6), 763-774.

669
670 Zhang, K.,Wu,Y.S., Pruess, K. (2008). User's guide for TOUGH2-MP- a massively parallel version
671 of the TOUGH2 code (No. LBNL– 315E). Ernest Orlando Lawrence Berkeley National Laboratory
672 Zaputlyaeva, A., Mazzini, A., Blumenberg, M., Scheeder, G., Kürschner, W. M., Kus, J., T.J.
673 Morgan & Frieling, J. (2020). Recent magmatism drives hydrocarbon generation in north-east Java,
674 indonesia. Scientific reports, 10(1), 1-14.
675
676 Zoporowski, A. & Miller, S. A. (2009). Modelling eruption cycles and decay of mud
677 volcanoes. Marine and Petroleum Geology, 26(9), 1879-1887.

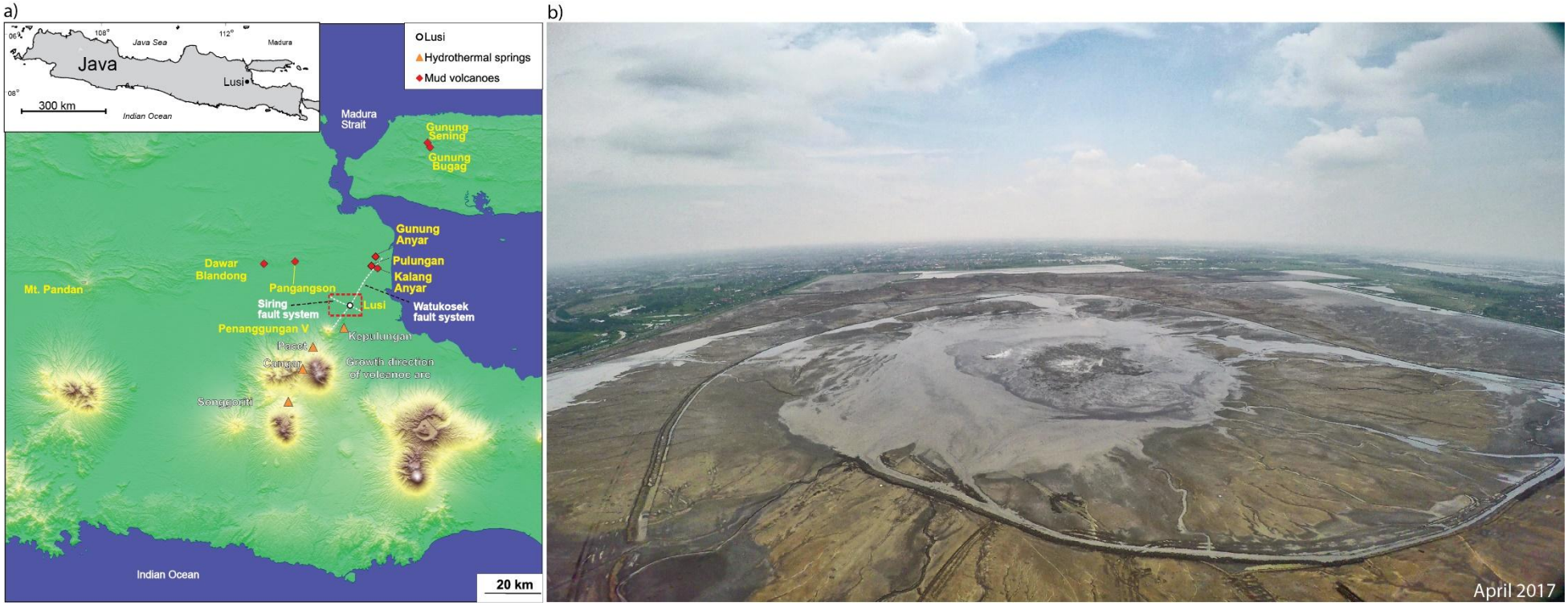
a)
b)
Java
Java Sea
Madura
Lusi
300 km
Indian Ocean
Lusi
Hydrothermal springs
Mud volcanoes
Madura Strait
Gunung Sening
Gunung Bugag
Gunung Anyar
Pulungan
Kalang Anyar
Dawar Blandong
Mt. Pandan
Pangangson
Siring fault system
Lusi
Watukosek fault system
Penanggungan V
Kepulungan
Pacet
Welirang
Growth direction of volcanoe arc
Semeru
Indian Ocean
20 km
April 2017

Figure 1

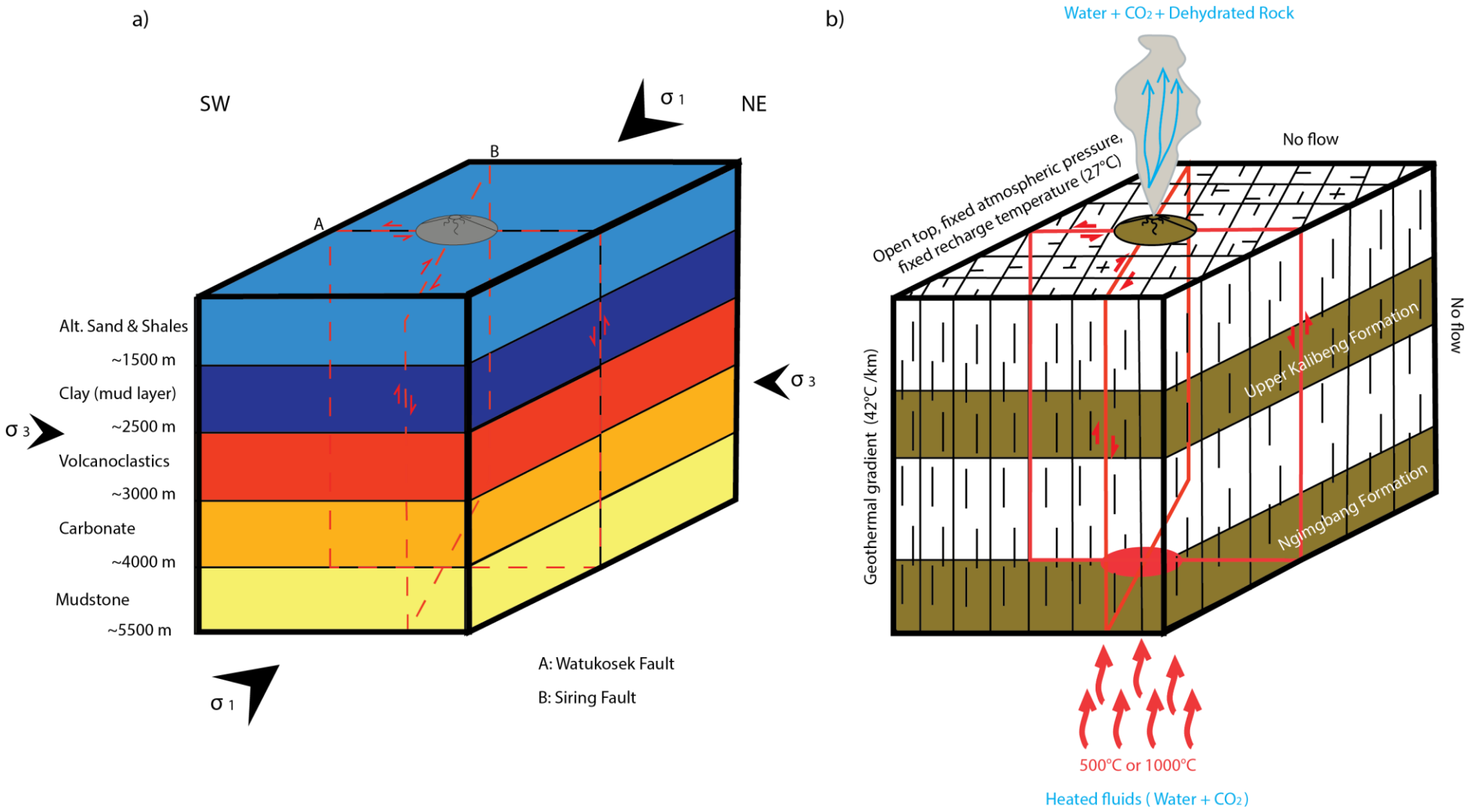
a)
SW
NE
σ 1
σ 3
B
A
Alt. Sand & Shales
~1500 m
Clay (mud layer)
~2500 m
Volcanoclastics
~3000 m
Carbonate
~4000 m
Mudstone
~5500 m
A: Watukosek Fault
B: Siring Fault
b)
Water + CO2 + Dehydrated Rock
No flow
Open top, fixed atmospheric pressure, fixed recharge temperature (27°C)
Geothermal gradient (42°C /km)
Upper Kalibeng Formation
Ngimgbang Formation
No flow
500°C or 1000°C
Heated fluids (Water + CO2)

Figure 2

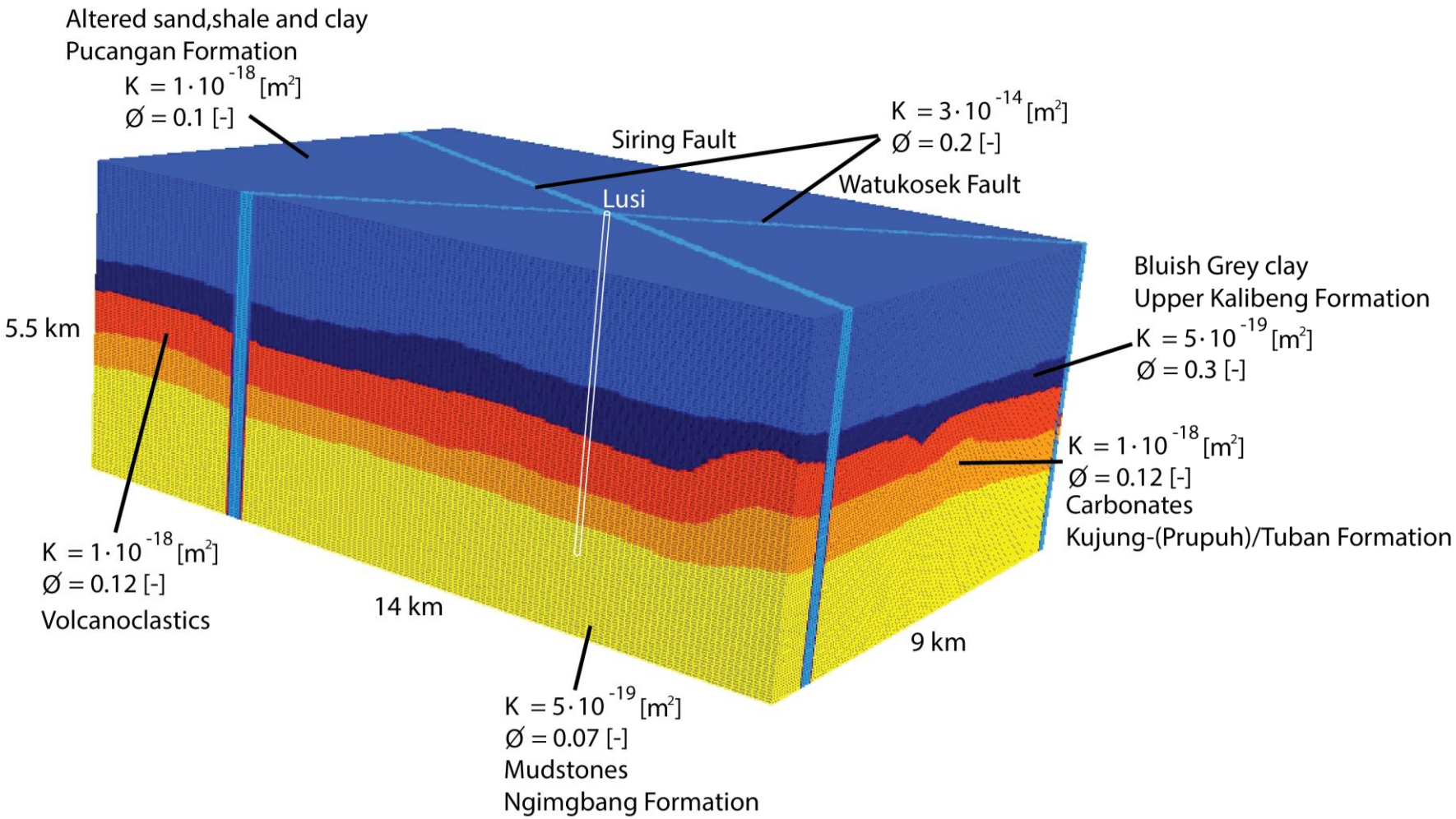
Altered sand,shale and clay
Pucangan Formation
K = 1·10 -18 [m²]
Ø = 0.1 [-]
Siring Fault
K = 3·10 -14 [m²]
Ø = 0.2 [-]
Watukosek Fault
Lusi
Bluish Grey clay
Upper Kalibeng Formation
K = 5·10 -19 [m²]
Ø = 0.3 [-]
5.5 km
K = 1·10 -18 [m²]
Ø = 0.12 [-]
Carbonates
Kujung-(Prupuh)/Tuban Formation
K = 1·10 -18 [m²]
Ø = 0.12 [-]
Volcanoclastics
14 km
9 km
K = 5·10 -19 [m²]
Ø = 0.07 [-]
Mudstones
Ngimgbang Formation

Figure 3

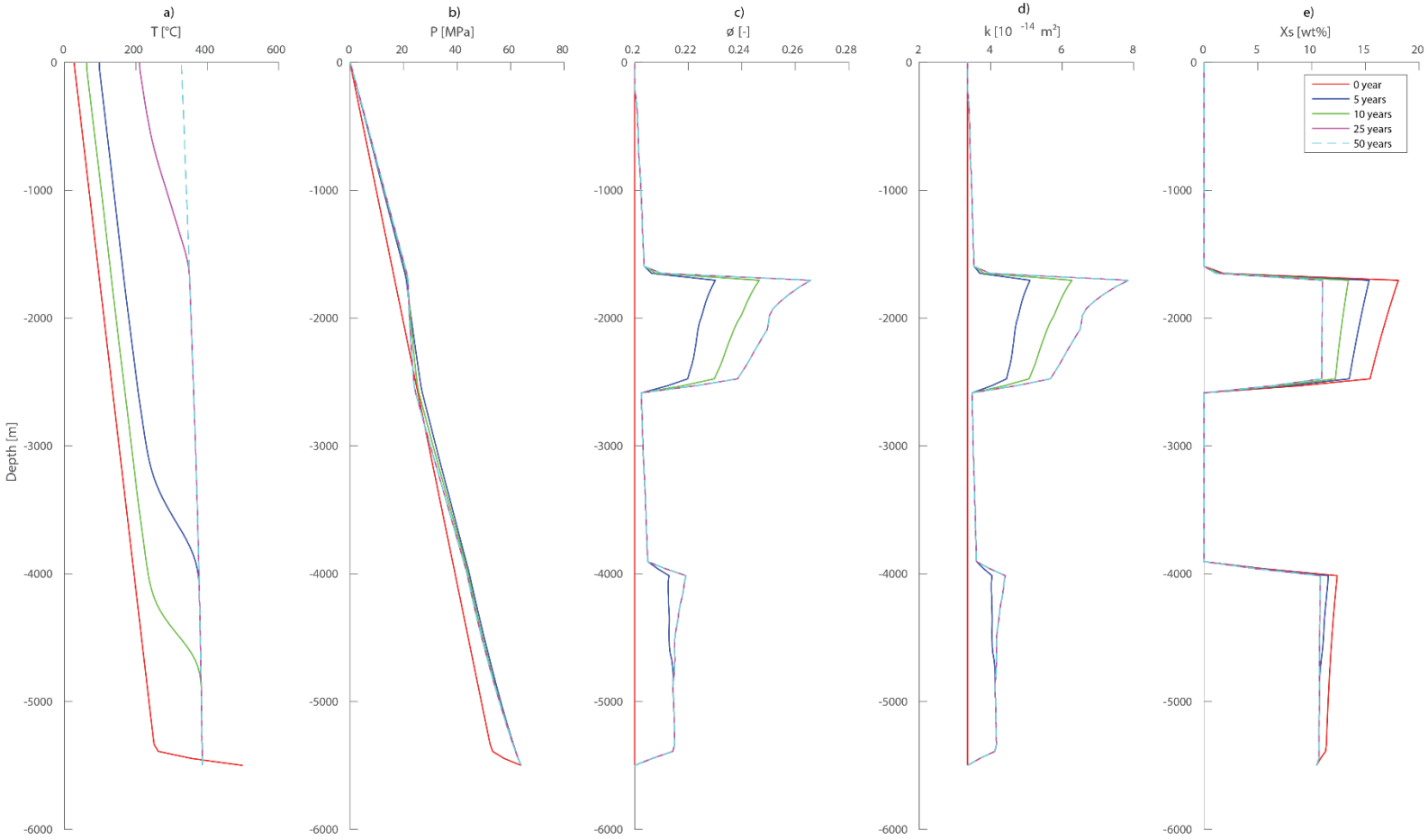
a)
T [°C]
b)
P [MPa]
c)
ø [-]
d)
k [10 -14 m2]
e)
Xs [wt%]
Depth [m]
0 year
5 years
10 years
25 years
50 years

685

Figure 4

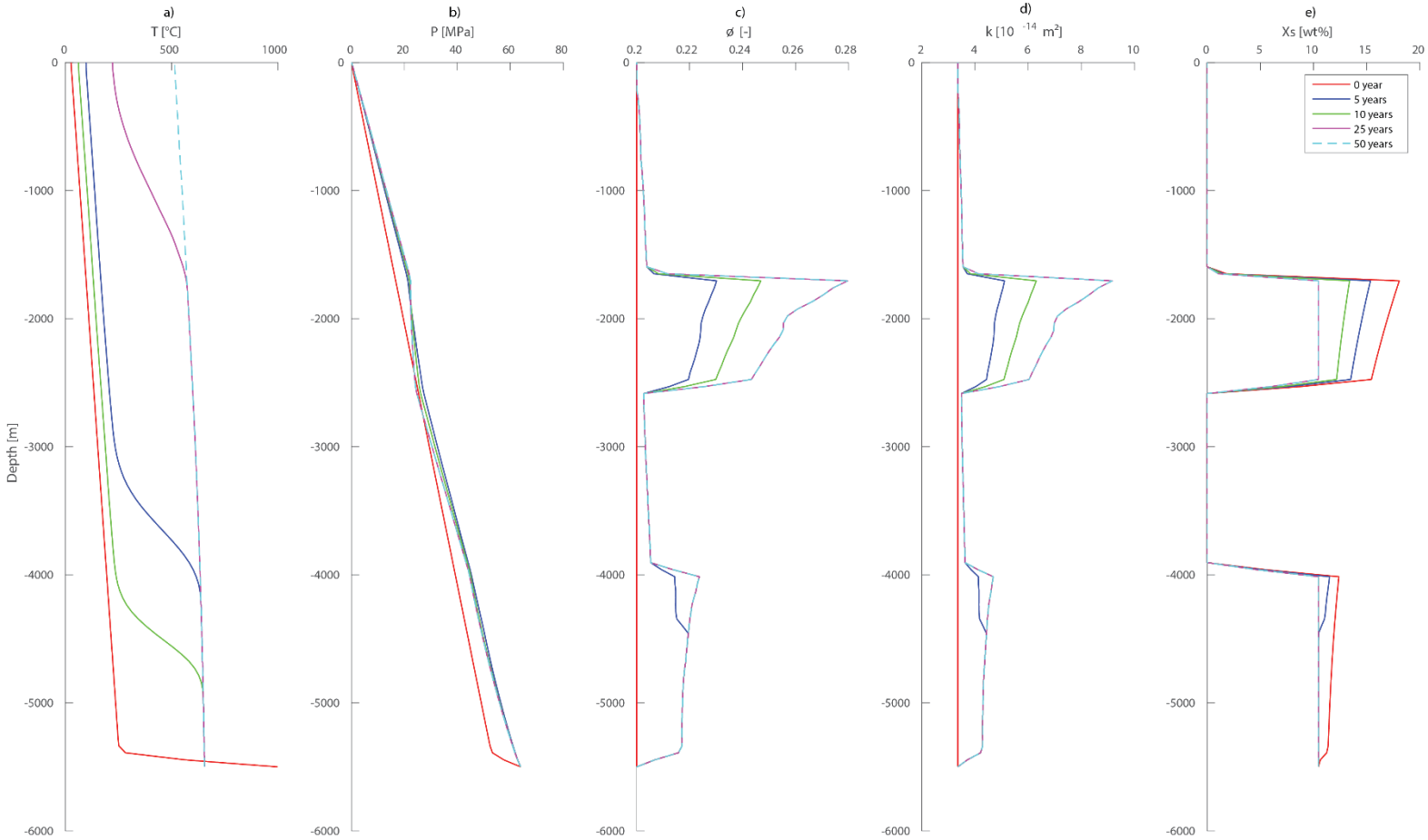
a)
T [°C]
b)
P [MPa]
c)
ø [-]
d)
k [10 -14 m2]
e)
Xs [wt%]
Depth [m]
0 year
5 years
10 years
25 years
50 years

Figure 5

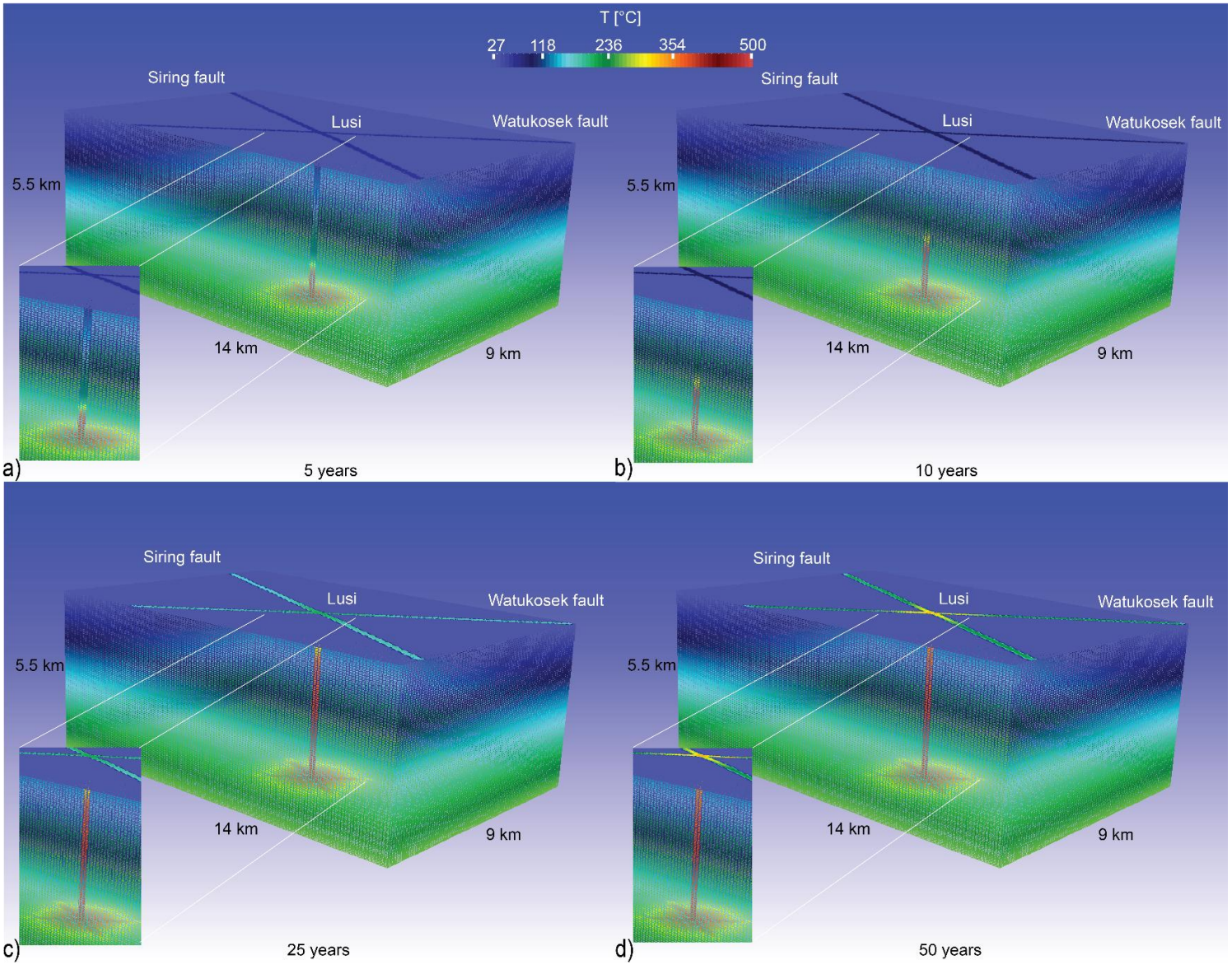
T [°C]
27 118 236 354 500
Siring fault
Lusi
Watukosek fault
5.5 km
14 km
9 km
a)
5 years
b)
10 years
c)
25 years
d)
50 years

Figure 6

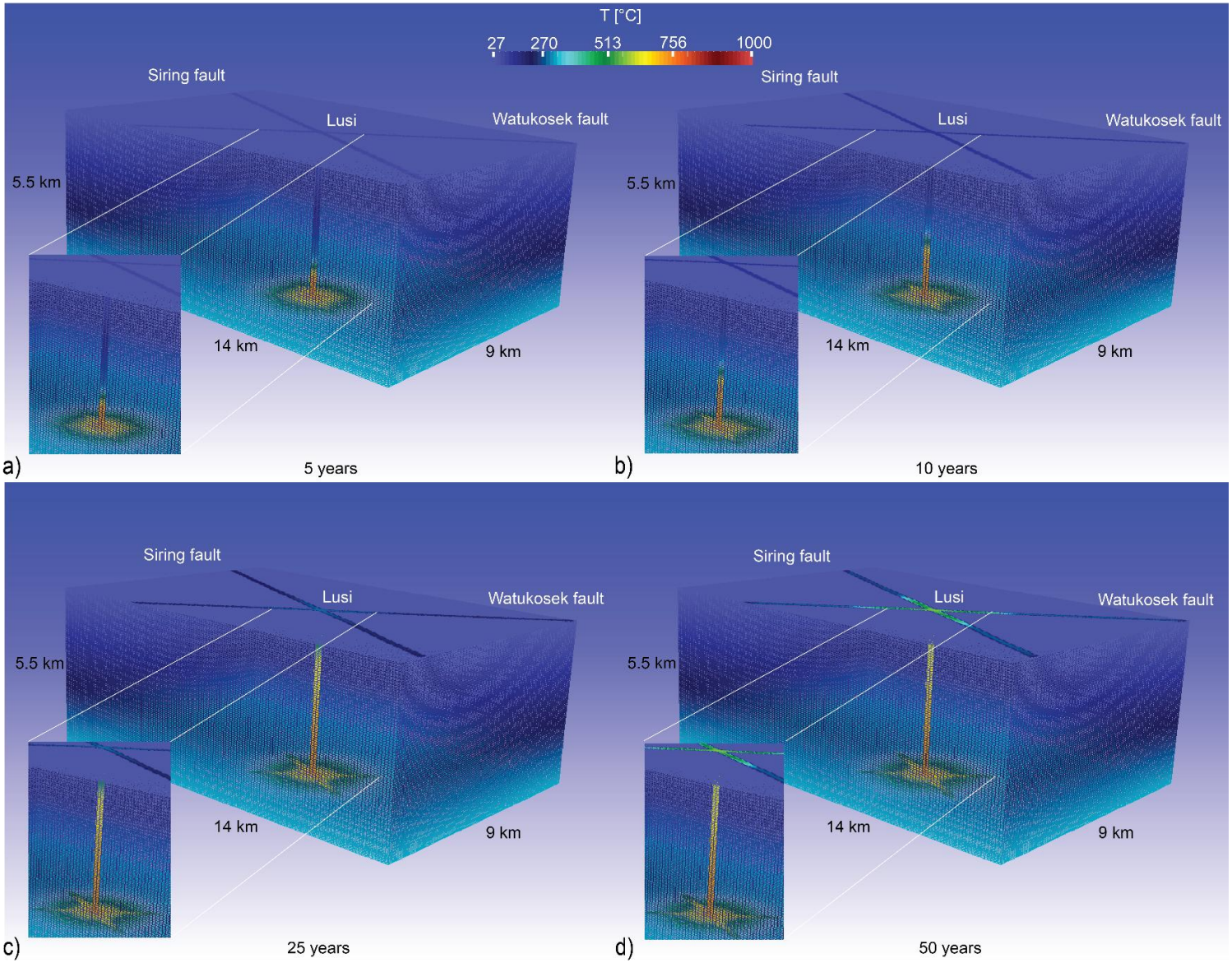
T [°C]
27 270 513 756 1000
Siring fault
Lusi
Watukosek fault
5.5 km
14 km
9 km
a)
5 years
b)
10 years
c)
25 years
d)
50 years

Figure 7

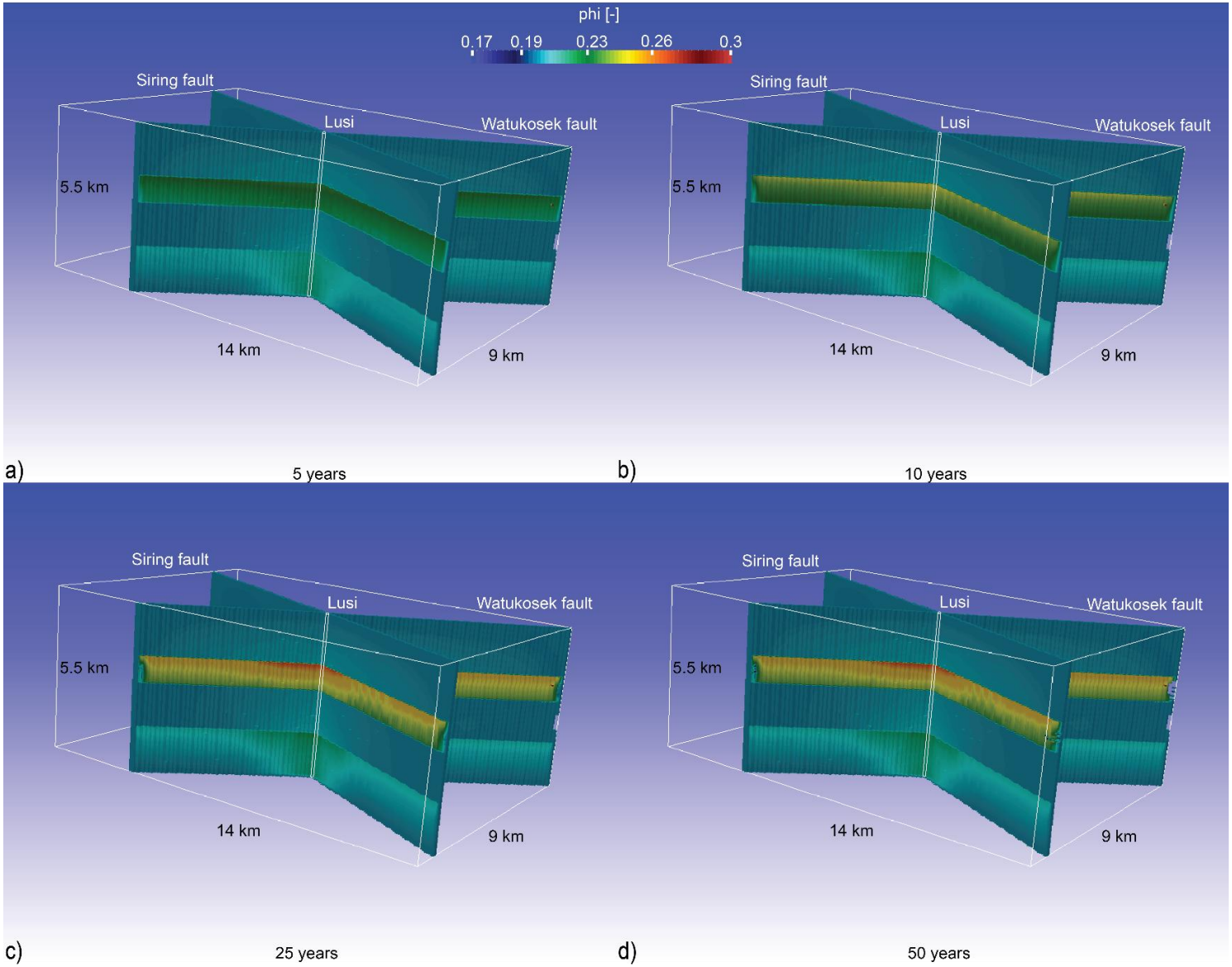
phi [-]
0.17 0.19 0.23 0.26 0.3
Siring fault
Lusi
Watukosek fault
5.5 km
14 km
9 km
a)
5 years
b)
10 years
c)
25 years
d)
50 years

Figure 8

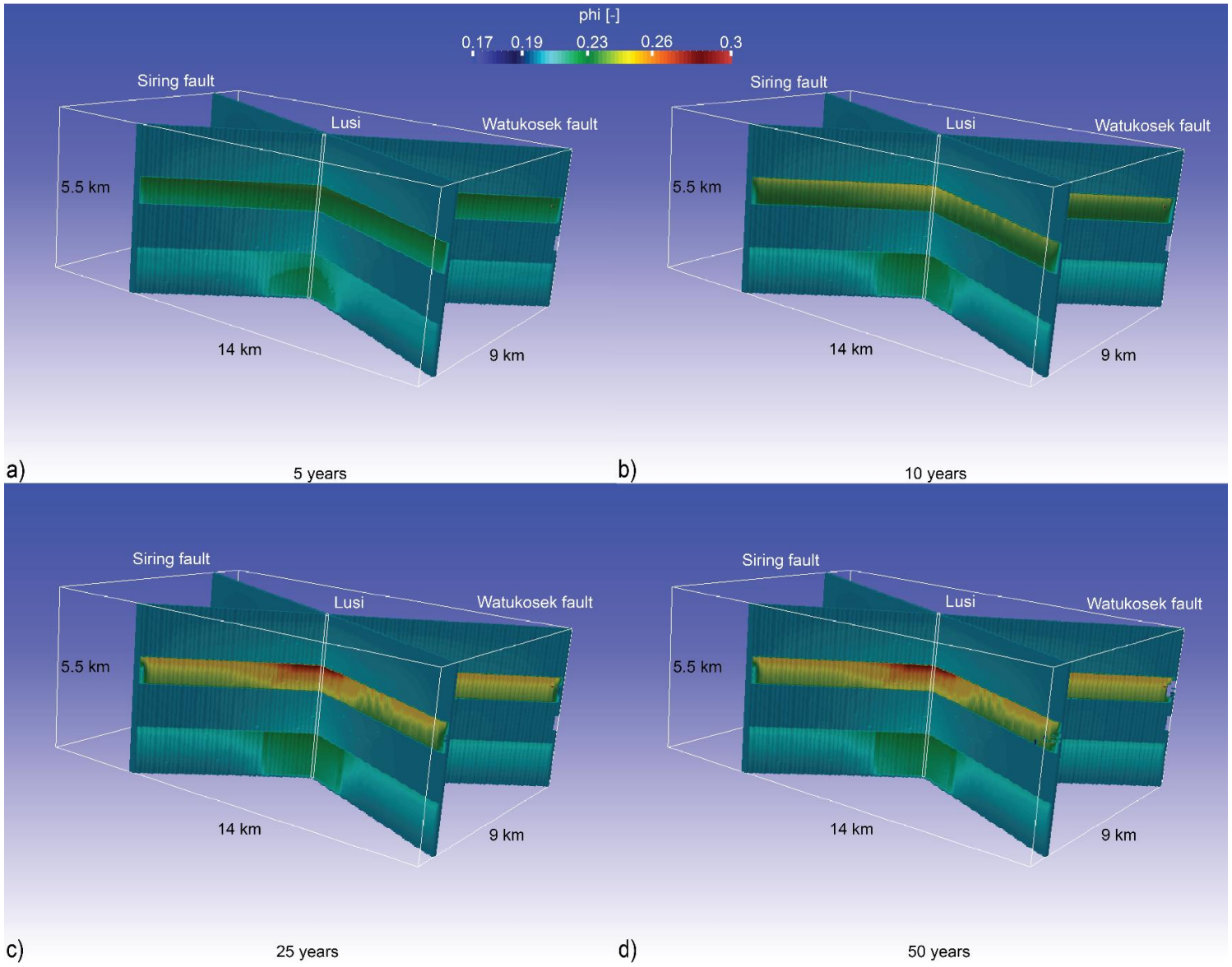
phi [-]
0.17 0.19 0.23 0.26 0.3
Siring fault
Lusi
Watukosek fault
5.5 km
14 km
9 km
a)
5 years
b)
10 years
c)
25 years
d)
50 years

Figure 9

695

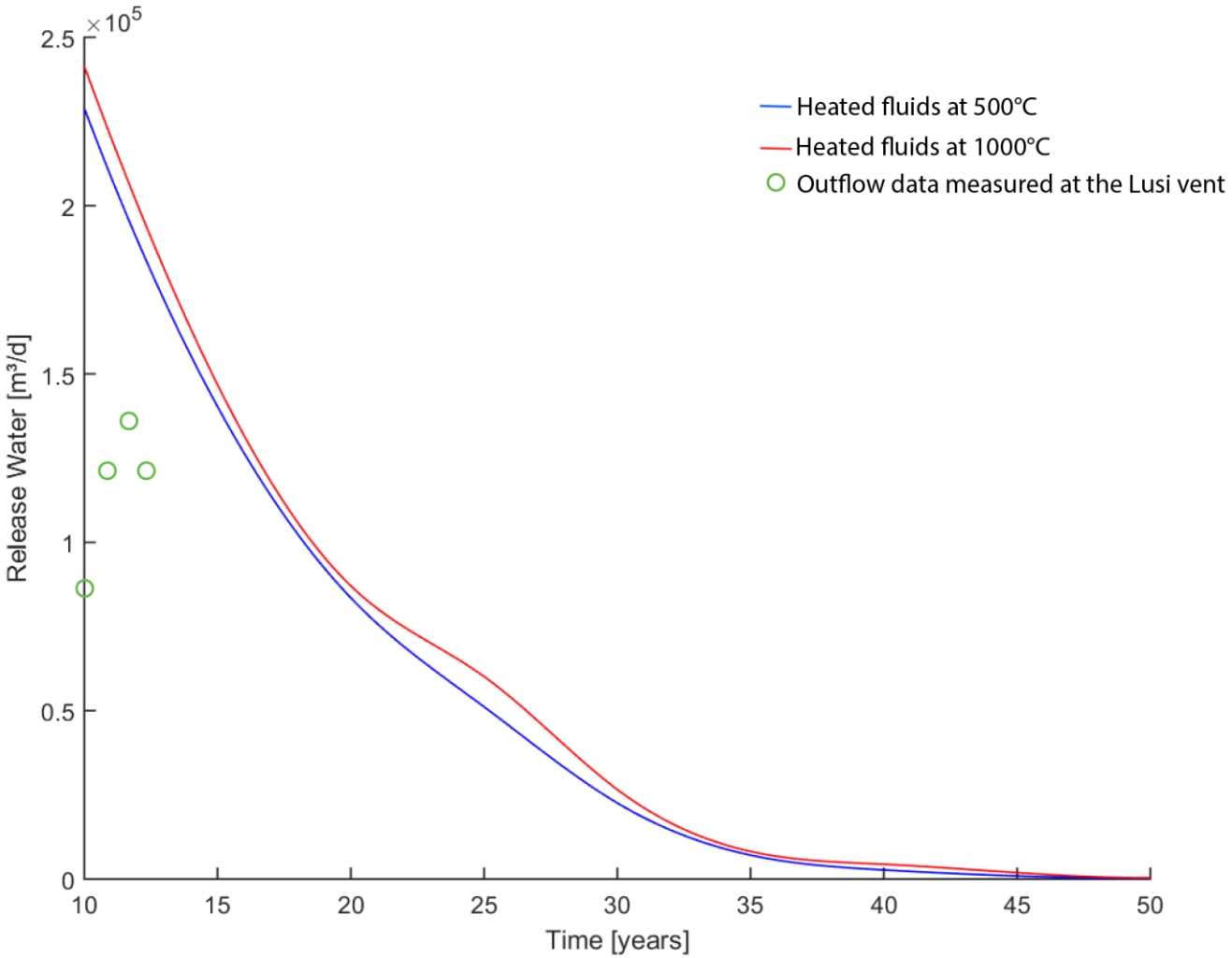

Figure 10

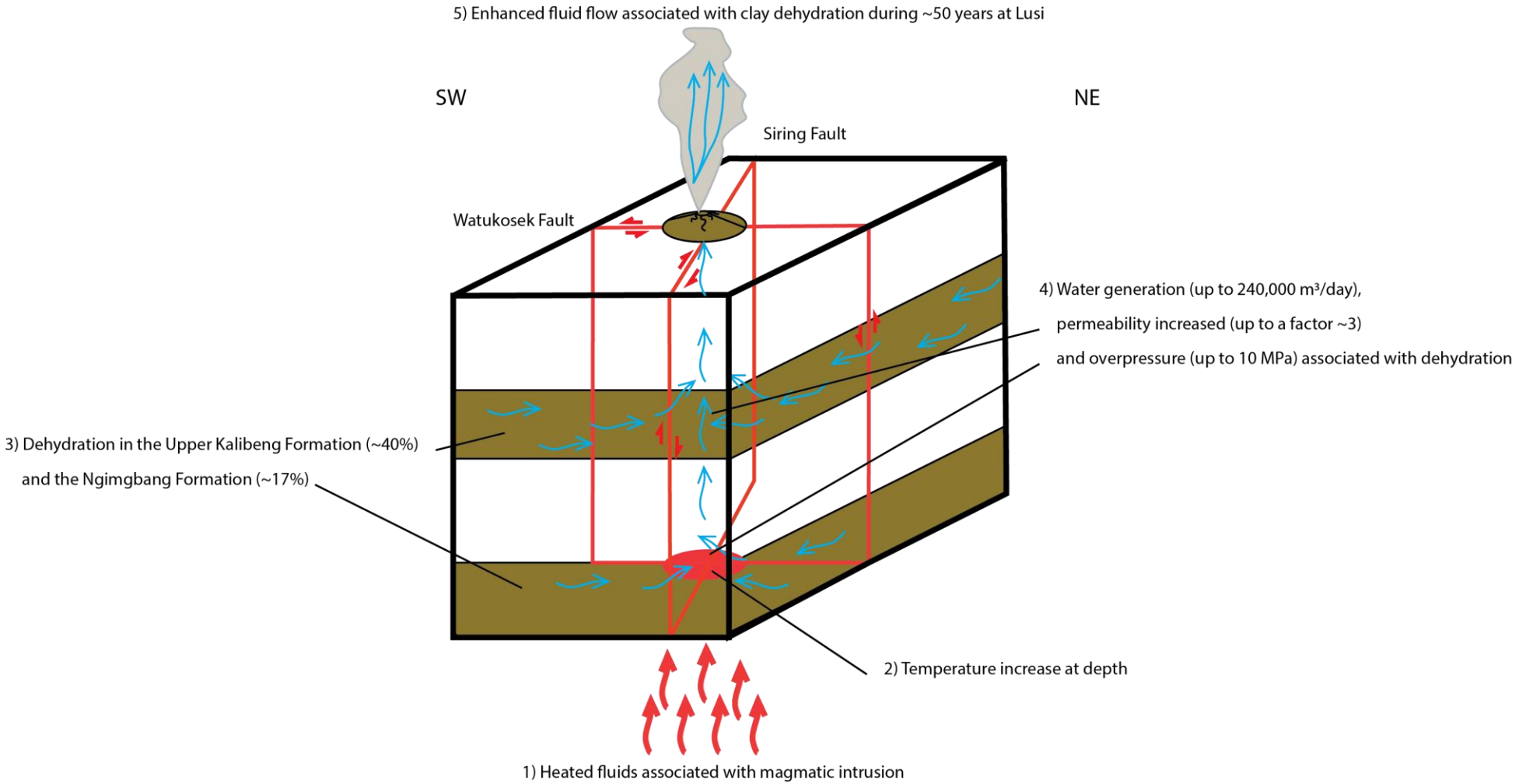

700

Figure 11